PTEP

Prog. Theor. Exp. Phys. **2022** 073C01(20 pages)
DOI: 10.1093/ptep/ptac090

Full electroweak $\mathcal{O}(\alpha)$ corrections to Higgs-boson production processes with beam polarization at the International Linear Collider

Nhi My Uyen Quach[1,2], Junpei Fujimoto[1,2], and Yoshimasa Kurihara[1,2]

[1]*High Energy Accelerator Research Organization (KEK), Tsukuba, Ibaraki 305-0801, Japan*
[2]*The Graduate University for Advanced Studies (SOKENDAI), Hayama, Kanagawa 240-0193, Japan*
*E-mail: junpei.fujimoto@kek.jp

Received April 28, 2022; Revised June 15, 2022; Accepted June 21, 2022; Published June 25, 2022

We present the full $\mathcal{O}(\alpha)$ electroweak radiative corrections to the production of nine Higgs bosons with beam polarization at the International Linear Collider (ILC). The computation is performed with the help of GRACE-Loop. We compare the full $\mathcal{O}(\alpha)$ electroweak radiative corrections with the factorized initial-state radiation (ISR) effects to estimate the pure weak corrections. This reveals that the pure weak corrections are not negligible and should be taken into account for precision measurements of the Higgs-boson property at the ILC experiments.

Subject Index B50, B53, B57, C21, C31

1. Introduction

The International Linear Collider (ILC) is a future linear electron–positron collider, operating at 250 to 500 GeV center-of-mass energies with high luminosity that can be extended to 1 TeV in the upgrade stage. It is based on 1.3 GHz superconducting radio-frequency (SCRF) accelerating technology [1,2]. The ILC is proposed to be constructed in the Kitakami Mountains in the Tohoku area, Japan. It is an international project that has been running for more than 20 years as a collaboration between more than 300 institutes, universities, and laboratories.

The major physics aim of the ILC is to determine the future direction of particle physics via precise measurements of the couplings of the Higgs boson with other elementary particles. A wide variety of elementary particles and nuclear physics can be studied.

On July 4, 2012, the Higgs-boson discovery was announced by physicists from two experiments (the CMS group and the ATLAS group) of the LHC at CERN. A new particle with a mass of approximately 125 GeV and several other properties of the Higgs boson, as predicted by the SM, was described in Refs. [3,4]. The Higgs-boson discovery made the SM of particle physics complete.

The prediction of additional Higgs bosons is one of the prominent features of possible physics of beyond the standard model, BSM, which leads to an extended Higgs-boson sector. Searching for higher-mass Higgs bosons is also very interesting. However, the hypothesis that the Higgs boson is heavy and approaches the theoretical upper bound has been validated by the expected exclusion regions with 300 fb^{-1} and 3 ab^{-1} LHC data. Therefore, the ILC is an exemplary collider to study the 125 GeV Higgs boson.

Funded by SCOAP[3]

With this Higgs particle, the first course at the ILC would be at threshold around $\sqrt{s} = 250$ GeV, which displays the clear peak cross section for the process $e^+e^- \to ZH$. At this energy, the precise measurements of the Higgs recoil mass for the Higgs-strahlung process $e^+e^- \to ZH$ with subsequent $Z \to l^+l^-(l = e, \mu)$ decay is one of the most important measurements. This measurement allows a model-independent absolute measurement of the g_{HZZ} coupling. In this setting, it is possible to measure the proportion for all Higgs-boson decays including common final states and invisible decays with great accuracy.

It is not necessary to observe Higgs decay because the corresponding hidden decay is observable. Nevertheless, the $e^+e^- \to ZH$ process can be used to measure diverse branching ratios for various Higgs decay processes. The $Z \to q\bar{q}$ and $Z \to \nu\bar{\nu}$ processes are included in this analysis to increase the statistics. The Higgs boson can also decay into a pair of W bosons. However, the measurement of the WW-fusion process at $\sqrt{s} = 250$ GeV is quite difficult. Conversely, the W-pair production process becomes active at $\sqrt{s} = 500$ GeV, and hence the energy setting of the ILC is expected to be changed accordingly [2].

In this paper, we study nine processes of $e^+e^- \to f\bar{f}H$ with polarized electron and positron beams of a center-of-mass energy at 250 GeV, i.e., the production of (1) a muon pair and a Higgs boson, (2) an electron–positron pair and a Higgs boson, (3) a tau pair and a Higgs boson, (4) a muon–neutrino pair and a Higgs boson, (5) an electron–neutrino pair and a Higgs boson, (6) an up-quark pair and a Higgs boson, (7) a down-quark pair and a Higgs boson, (8) a charm-quark pair and a Higgs boson, and (9) a bottom-quark pair and a Higgs boson (note that we do not consider the production of top-quark, strange-quark, or tau-neutrino pairs). We calculate the $\mathcal{O}(\alpha)$ corrections using the on-shell renormalization scheme to each of these nine reactions as well as the one-photon emission process.

In this work, we have used the GRACE-Loop system to calculate the amplitudes automatically. We have developed two sets of Fortran codes.

The first set was used to calculate the $O(\alpha)$ corrections corresponding to the one-loop diagrams and the one-photon emission processes; in this case, all the fermion masses were kept non-zero, except for the neutrino masses, and arbitrary longitudinal polarization of the input electron and positron beams was available. The second set was used to treat the effects of initial-state radiation (ISR). The effects of one-loop weak corrections were determined by comparing the $O(\alpha)$ corrections with the ISR effects.

We introduce the NOLFS (no light-fermion scalar coupling) approximation, where the couplings between the light fermions (except for bottom and top quarks) and scalar particles are neglected, but the masses of all fermions are retained. We confirmed the one-loop amplitudes generated using the NOLFS approximation to be consistent with those obtained from the Monte Carlo integration of the full Lagrangian. Therefore, in this work, we present and discuss the results obtained using the NOLFS approximation.

The structure of this paper is as follows; after the introduction, we will explain the calculation framework of GRACE-Loop in Sect. 2. In Sect. 3, we will define the beam polarization of the ILC beams. The recoil mass analysis is introduced in Sect. 4. In Sect. 5, we will explain the radiator method of the initial-state radiation. Then we will present the numerical results for the leptonic processes in Sect. 6 and those for the quark processes in Sect. 7. Section 8 discusses the recoil mass distribution of $e^+e^- \to \mu^+\mu^-H$. Finally we will give a discussion in Sect. 9, and Sect. 10 is devoted to the conclusion of this paper.

Table 1. The numbers of Feynman diagrams for the NOLFS approximation and the FULL model for nine processes.

	NOLFS approximation			FULL model		
Graph information	One-loop	Tree	Five-point	One-loop	Tree	Five-point
$\mu^+\mu^- H$	208	1	10	2235	21	170
$e^+e^- H$	416	2	20	4470	42	340
$\tau^+\tau^- H$	208	1	28	2235	21	188
$\nu_\mu\bar{\nu}_\mu H$	122	1	6	604	4	36
$\nu_e\bar{\nu}_e H$	219	2	15	1350	12	113
$u\bar{u}H$	209	1	10	2327	21	174
$d\bar{d}H$	209	1	10	2327	21	174
$c\bar{c}H$	209	1	10	2327	21	174
$b\bar{b}H$	651	6	29	2327	21	193

2. GRACE-Loop and the calculation of $e^+e^- \to f\bar{f}H$

The GRACE-Loop system is a programming system for calculating full one-loop electroweak cross sections and the tree level automatically, with beam polarizations based on the SM and minimal supersymmetric standard model (MSSM) of high-energy physics. This program was created and developed by the Minami-Tateya group at the High Energy Accelerator Research Organization, KEK [5]. It uses the symbolic manipulation system FORM [6] to calculate all Dirac and tensor algebra in n dimensions.

In the GRACE system [5], at the tree level, beam polarization effects are taken into account from the beginning to produce helicity amplitudes, which are evaluated numerically. Nevertheless, at the full one-loop electroweak corrections with the GRACE-Loop system, it adopts trace techniques to get the interference between the tree amplitudes and one-loop ones using symbolical manipulation with the FORM system. Then, the polarization effects of the beams are included with the insertion of the projection operators, $\frac{1\pm\gamma_5}{2}$, into amplitudes. This makes the program much larger.

This has been successfully tested for a variety of one-loop $2 \to 2$ electroweak processes [7]. It also provided the first results on the full one-loop radiative corrections to $e^+e^- \to \nu\bar{\nu}H$ [8], which have been confirmed by an independent calculation [9].

The GRACE-Loop system primarily focuses on evaluating one-loop corrections to the SM processes during electron–positron collisions. In addition, it can calculate one-loop corrections to the MSSM [10].

It should be noted the FULL model contains all of the couplings of the scalar particles such as the Higgs boson or pseudo-Goldstone scalar bosons and fermions in the SM are included.

In this paper, bottom and top quarks are considered to be heavy fermions and other fermions are recognized as light ones.

When the two cases of the FULL model and the NOLFS approximation are compared, the number of tree diagrams and one-loop Feynman diagrams in the former is much larger than in the latter; thus, integration over phase space is not practical in the former, as shown in Table 1.

From Table 1, we observe that the number of one-loop Feynman diagrams of the $\mu^+\mu^- H$ and $\tau^+\tau^- H$ processes is the same, with 208 and 2235 diagrams with the NOLFS approximation and the FULL model, respectively. Similarly, the number of one-loop Feynman diagrams of the $u\bar{u}H$, $d\bar{d}H$, and $c\bar{c}H$ processes is the same, with 209 and 2327 diagrams according to

Table 2. Changing $C_{\rm UV}$ from 0 to 100 for $e^+e^- \to \mu^+\mu^- H$ of the FULL model at a phase point in arbitrary units with $k_c = 10^{-1}$ GeV, $\lambda = 10^{-17}$ GeV, and $\Gamma_Z = 0$ GeV at $\sqrt{s} = 250$ GeV.

$C_{\rm UV}$	Evaluation of the one-loop amplitude
0	0.127 132 019 079 521 763 060 824 923 741 166
100	0.127 132 019 079 521 763 060 824 923 741 166

Table 3. λ independence of $e^+e^- \to \mu^+\mu^- H$ of the FULL model at a phase space point in arbitrary units by changing from 10^{-17} GeV to 10^{-19} GeV with $C_{\rm UV} = 0$ at $\sqrt{s} = 250$ GeV and $\Gamma_Z = 0$ GeV.

λ [GeV]	Evaluation of the one-loop amplitude
10^{-17}	0.127 132 019 079 521 763 060 824 923 741 166
10^{-19}	0.127 132 019 079 522 845 528 273 933 268 792

the one-loop level with the NOLFS approximation and the FULL model, respectively. However, the number of Feynman diagrams of the one-loop level of $b\bar{b}H$ is 651 with the NOLFS approximation and 2327 with the FULL model.

For all electroweak processes we adopt the on-shell renormalization scheme according to Refs. [7,11]. The one-loop scalar integrals with the width are evaluated using the LoopTools packages [12]; on the other hand, the detail of the reduction on the tensor integrals and the five-point functions based on the Feynman parameters are described in Ref. [7].

The matrix elements to the electroweak corrections produced by the GRACE-Loop are checked by performing three kinds of tests at a random point in phase space. For these tests to be passed one works in quadruple precision.

We first have to check the ultraviolet finiteness of the results. This test applies to the whole set of virtual one-loop diagrams. In order to conduct this test we regularize any infrared divergence by giving the photon a fictitious mass (we set this at $\lambda = 10^{-15}$ GeV). In the intermediate step of the symbolic calculation dealing with loop integrals (in n dimensions), we extract the regulator constant $C_{\rm UV} = 1/\varepsilon - \gamma_E + \log 4\pi$, $n = 4 - 2\varepsilon$ and treat this as a parameter. The ultraviolet finiteness test is performed by varying the dimensional regularization parameter $C_{\rm UV}$. This parameter could then be set to 0 in further computation.

By varying $C_{\rm UV}$ from 0 to 100 for the $e^+e^- \to \mu^+\mu^- H$ process of the FULL model with $k_c = 10^{-1}$ GeV, $\lambda = 10^{-17}$ GeV, and $\Gamma_Z = 0$ GeV at $\sqrt{s} = 250$ GeV, we obtained $C_{\rm UV}$ independence with an agreement up to 33 digits as shown in Table 2.

As the second test, the infrared finiteness was checked by including both loop and bremsstrahlung contributions and checking that there is no dependence on the fictitious photon mass λ.

Fictitious photon mass (λ) independence was achieved by varying λ from 10^{-17} GeV to 10^{-19} GeV with $C_{\rm UV} = 100$ and $\Gamma_Z = 0$ GeV, giving up to 14-digit agreement as shown in Table 3.

A crucial test concerns the gauge parameter independence of the results. This is performed through a set of five gauge fixing parameters. For the latter a generalized non-linear gauge

Table 4. Non-linear gauge parameter independence of the FULL model by changing $\tilde{\alpha}, \tilde{\beta}, \tilde{\delta}, \tilde{\kappa}, \tilde{\varepsilon}$ at a phase point in arbitrary units from (0,0,0,0,0) to (10,20,30,40,50) for $e^+e^- \to \mu^+\mu^- H$ with $k_c = 10^{-1}$ GeV, $\lambda = 10^{-17}$ GeV at $\sqrt{s} = 250$ GeV, and $\Gamma_Z = 0$ GeV.

$\tilde{\alpha}, \tilde{\beta}, \tilde{\delta}, \tilde{\kappa}, \tilde{\varepsilon}$	Evaluation of the one-loop amplitude
0,0,0,0,0	0.127 132 019 079 521 763 060 824 923 741 166
10,20,30,40,50	0.127 132 019 079 522 096 127 732 311 288 128

Table 5. Comparison of the one-loop amplitudes at a phase point between the FULL model and the NOLFS approximation in arbitrary units for $e^+e^- \to \mu^+\mu^- H$ with $k_c = 10^{-1}$ GeV at $\sqrt{s} = 250$ GeV and $\Gamma_Z = 0$ GeV in order to avoid the violation of the gauge invariance.

FULL model vs. NOLFS approximation	Evaluation of the one-loop amplitude
FULL model	0.127 132 019 079 521 763 060 824 923 741 166
NOLFS approximation	0.127 180 115 426 583 029 147 877 823 561 430

fixing condition [7,13] has been chosen:

$$\mathcal{L}_{\rm GF} = -\frac{1}{\xi_W}|(\partial_\mu - ie\tilde{\alpha}A_\mu - igc_W\tilde{\beta}Z_\mu)W^{\mu+} + \xi_W\frac{g}{2}(v+\tilde{\delta}H+i\tilde{\kappa}\chi_3)\chi^+|^2$$
$$-\frac{1}{2\xi_Z}(\partial.Z+\xi_Z\frac{g}{2c_W}(v+\tilde{\varepsilon}H)\chi_3)^2 - \frac{1}{2\xi_A}(\partial.A)^2. \quad (1)$$

The χ represent the Goldstones. We take the 't Hooft–Feynman gauge with $\xi_W = \xi_Z = \xi_A = 1$ so that no "longitudinal" term in the gauge propagators contributes. Not only does this make the expressions much simpler and avoids unnecessary large cancellations, but it also avoids the need for high tensor structures in the loop integrals. The use of the five parameters $\tilde{\alpha}, \tilde{\beta}, \tilde{\delta}, \tilde{\kappa}, \tilde{\varepsilon}$ is not redundant as often these parameters check complementary sets of diagrams.

Non-linear gauge parameter independence was confirmed by varying $\tilde{\alpha}, \tilde{\beta}, \tilde{\delta}, \tilde{\kappa}, \tilde{\varepsilon}$ from (0,0,0,0,0) to (10,20,30,40,50) with $C_{\rm UV} = 100$ at $\sqrt{s} = 250$ GeV and $\Gamma_Z = 0$ GeV in order to avoid the violation of the gauge invariance, which resulted in an agreement up to 15 digits as shown in Table 4.

We also show a comparison between the FULL model and the NOLFS approximation at a phase space point in Table 5.

An additional stability test on the NOLFS approximation concerns the bremsstrahlung part. It relates to the independence in the parameter k_c, which is a soft photon cut parameter that separates soft photon radiation and the hard photon performed by the Monte Carlo integration package of BASES [14]. Here, we have implemented the finite fixed width in all Z-boson propagators as $P_Z(q) = [q^2 - m_Z^2 + im_Z\Gamma_Z]^{(-1)}$ with $\Gamma_Z = 2.49$ GeV [15] in order to avoid hitting the pole of the Z-boson propagators in the amplitudes.

In the BASES operation, to integrate the one-loop amplitude, we set 10 iteration steps for the grid optimization and 200 iteration steps for the accumulation with 40 000 sampling points. It takes 16 h for $\mu^+\mu^- H$ and other processes, including almost 103 h for $b\bar{b}H$, with 16 Xeon 3.20 GHz CPUs with 128 GB memory. The typical integration errors are 0.06% for each step of the loop calculations. From Table 6, we claim that the accuracy of our $\mathcal{O}(\alpha)$ corrections is approximately 0.1% for all nine processes.

Table 6. $\delta_{\rm Total}$ in % with various k_c values of 10^{-1}, 10^{-3}, and 10^{-5} GeV for all nine processes without beam polarizations at $\sqrt{s} = 250$ GeV.

Process	$\delta_{\rm Total}(\%)$ $k_c = 10^{-1}$ GeV	$k_c = 10^{-3}$ GeV	$k_c = 10^{-5}$ GeV
$\mu^+\mu^- H$	−4.14(08)	−4.14(08)	−4.23(08)
$e^+e^- H$	−4.45(09)	−4.53(09)	−4.44(09)
$\tau^+\tau^- H$	−4.54(08)	−4.62(08)	−4.59(08)
$\nu_\mu\bar{\nu}_\mu H$	−4.37(13)	−4.40(14)	−4.45(16)
$\nu_e\bar{\nu}_e H$	−3.56(12)	−3.55(12)	−3.55(12)
$u\bar{u}H$	−6.75(10)	−6.75(10)	−6.70(10)
$d\bar{d}H$	−4.97(10)	−5.06(10)	−5.12(10)
$c\bar{c}H$	−6.41(10)	−6.39(10)	−6.46(10)
$b\bar{b}H$	−6.50(11)	−6.49(11)	−6.44(11)

Table 7. Comparison between the unpolarized cross sections of $e^+e^- \to \nu\bar{\nu}H$ for the current results and those of the German group [9] at $\sqrt{s} = 500$ GeV.

m_H (GeV)	m_W (GeV)	$\sigma_{\rm Tree}$ (pb)	$\sigma_{\mathcal{O}_\alpha}$ (pb)	$\delta_{\rm Total}\%$	
150	80.3767	$6.1072(9) \times 10^{-2}$	$6.075(6) \times 10^{-2}$	−0.5	Current
		$6.1076(5) \times 10^{-2}$	$6.080(2) \times 10^{-2}$	−0.4	Ref. [9]
200	80.3571	$3.7302(5) \times 10^{-2}$	$3.705(4) \times 10^{-2}$	−0.7	Current
		$3.7293(3) \times 10^{-2}$	$3.709(2) \times 10^{-2}$	−0.6	Ref. [9]
250	80.3411	$2.110(2) \times 10^{-2}$	$2.059(2) \times 10^{-2}$	−2.4	Current
		$2.1134(1) \times 10^{-2}$	$2.060(1) \times 10^{-2}$	−2.5	Ref. [9]
300	80.3275	$1.0744(7) \times 10^{-2}$	$1.0258(7) \times 10^{-2}$	−4.5	Current
		$1.075\,52(7) \times 10^{-2}$	$1.0282(4) \times 10^{-2}$	−4.4	Ref. [9]
350	80.3158	$4.6077(4) \times 10^{-3}$	$4.172(2) \times 10^{-3}$	−9.5	Current
		$4.6077(2) \times 10^{-3}$	$4.181(1) \times 10^{-3}$	−9.3	Ref. [9]

As a final check, in Table 7 we show a comparison between the unpolarized cross sections of $e^+e^- \to \nu\bar{\nu}H$ for the current results and those of the German group [9] at a center-of-mass energy of $\sqrt{s} = 500$ GeV because, in those days, the Higgs boson had not yet been confirmed.

3. Beam polarization

Here we would like to define the beam polarization and the realistic polarization status of the proposed ILC. The left-handed polarization degree of the electron beam is defined as

$$p_e = (N_{e_R} - N_{e_L})/(N_{e_L} + N_{e_R}), \tag{2}$$

where N_{e_R} and N_{e_L} are the numbers of right-handed and left-handed electrons in the beam, respectively, and

$$p_p = (N_{p_R} - N_{p_L})/(N_{p_R} + N_{p_L}), \tag{3}$$

where N_{p_R} and N_{p_L} are the numbers of right-handed and left-handed positrons in the beam, respectively.

When a normalization $N_L + N_R = 1$ is used, the normalized number of left-handed and right-handed electrons can be obtained as $N_L = \frac{1-p_e}{2}$ and $N_R = \frac{1+p_e}{2}$, respectively.

Therefore, the cross sections for a given combination of the electron and positron beam polarization can be written as:

$$\sigma(p_e, p_p) = \frac{1}{4}\{(1-p_e)(1+p_p)\sigma_{LR} + (1+p_e)(1-p_p)\sigma_{RL} + (1-p_e)(1-p_p)\sigma_{LL} + (1+p_e)(1+p_p)\sigma_{RR}\} \quad (4)$$

where σ_{LR} stands for the cross section with 100% left-handed polarized electron ($p_e = -1$) and 100% right-handed polarized positron ($p_p = +1$) beams. The cross sections σ_{RL}, σ_{LL}, and σ_{RR} are defined analogously.

The proposed ILC polarizations of the design values are

$$p_e = \frac{0.1 - 0.9}{1} = -0.8 \quad (5)$$

and

$$p_p = \frac{0.65 - 0.35}{1} = 0.3. \quad (6)$$

In subsequent discussions, we use the following short notations for the various polarization conditions:

- $p_e = 0, p_p = 0$ UP: unpolarized,
- $p_e = +1, p_p = +1$ RR: right e^- right e^+,
- $p_e = -1, p_p = -1$ LL: left e^- left e^+,
- $p_e = +1, p_p = -1$ RL: right e^- left e^+,
- $p_e = -1, p_p = +1$ LR: left e^- right e^+,
- $p_e = -0.8, p_p = 0.3$ ILC: the proposed ILC polarization.

4. Recoil mass analysis

We introduce the recoil mass analysis that we conducted to make a model-independent measurement of the coupling between the Higgs and Z bosons (i.e., g_{HZZ} coupling), using the recoil mass distribution in $e^+e^- \to ZH$ with $Z \to \mu^+\mu^-$ [16].

In electron–positron collisions at $\sqrt{s} = 250$ GeV, the main Higgs production mechanism is the Higgs-strahlung process $e^+e^- \to HZ$. For $m_H = 125$ GeV, the cross section for the s-channel process is maximal close to $\sqrt{s} = 250$ GeV.

The total HZ cross section is proportional to the square of the coupling between Higgs and Z bosons, i.e., $\sigma(e^+e^- \to HZ) \propto g^2_{HZZ}$, and the cross sections of the decays to the final state in $H \to X\bar{X}$ can be expressed as

$$\sigma(e^+e^- \to HZ) \times BR(H \to X\bar{X}) \propto \frac{g^2_{HZZ} \times g^2_{HXX}}{\Gamma_H}.$$

In this study, the cross section of $e^+e^- \to HZ$ was measured using the recoil mass technique. We considered $\sigma(e^+e^- \to HZ)$, and the recoil mass can be expressed as

$$m^2_{\text{rec}} = s - 2\sqrt{s}(E_{\mu^+} + E_{\mu^-}) + m^2_{\mu^+\mu^-}, \quad (7)$$

where $\sqrt{s}$ is the center-of-mass energy, E_{μ^+} and E_{μ^-} are the energies of the two muons, and $m^2_{\mu^+\mu^-}$ is the invariant mass of the muon and anti-muon from Z decay.

At $\sqrt{s} = 250$ GeV, where the energy of the muons from Z decay approximately scales as $\sqrt{s}$, the width of the recoil mass distribution increases significantly with increasing center-of-mass energy. Therefore, the leptonic (in particular, muonic) recoil mass analysis leads to a higher precision on g_{HZZ} for $\sqrt{s} = 250$ GeV, where $\sigma(HZ)$ is largest and the recoil mass peak is relatively

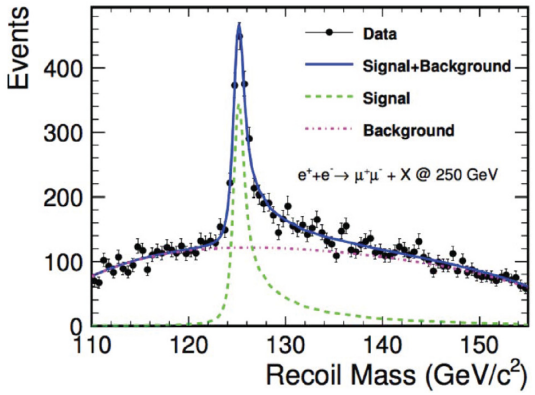

Fig. 1. Recoil mass distribution of the Higgs-strahlung process $e^+e^- \to \mu^+\mu^- H$ ($e^+e^- \to ZH$ followed by $Z \to \mu^+\mu^-$) with 250 fb^{-1} for $m_h = 120$ GeV at $\sqrt{s} = 250$ GeV [16].

narrow. Using this technique, one can determine the absolute branching ratios of Higgs-boson decays, including those of the invisible decays. It should be noted that, in this recoil mass distribution, simple ISR and detector resolution effects are included, leading to the appearance of the tail structure in Fig. 1.

The International Linear Collider (ILC) is a proposed international e^+e^- linear collider with beam energies ranging from 250 GeV to 1 TeV. ILC is supposed to start at a center-of-mass energy of 250 GeV in its initial stage to obtain high statistics measurements of the Higgs boson. Note that this center-of-mass energy was used for the calculations in this paper.

Owing to parity violation in weak interactions, beam polarization effects are essential to resolve new phenomena beyond the standard model (BSM); hence, studying these effects is necessary. Beam polarization and its importance in studying physics at the e^+e^-collider have been discussed in detail in recent decades. A precise measurement to study the properties of the Higgs boson is one of the key targets of the ILC experiments. However, to achieve this, one needs to know the $\mathcal{O}(\alpha)$ corrections to the underlying processes.

5. Radiator method

The effect of the initial photon emission can be factorized when the total energy of the emitted photons is sufficiently small compared to the beam energy or for small-angle (collinear) emissions. This approximation is referred as to the soft–collinear photon approximation (SPA). Under SPA, the corrected cross sections with ISR, i.e., $\sigma_{\rm ISR}$, can be obtained from the tree cross sections $\sigma_{\rm Tree}$ using a radiator function $H(x, s)$ as follows:

$$\sigma_{\rm ISR} = \int_0^1 dx\, H(x,s)\sigma_{\rm Tree}\left(s(1-x)\right), \tag{8}$$

where s is the square of the CM energy and x is the energy fraction of an emitted photon.

The total cross section with higher-order QED corrections to ISR can be calculated using the following function [17]:

$$\sigma_{\rm ISR} = \int_0^{k_c^2/s} dx_1 \int_0^{1-x_1} dx_2\, D(x_1,s)D(x_2,s)\sigma_{\rm Tree}\left(sx_1x_2\right), \tag{9}$$

where the structure function $D(x, s)$, which corresponds to the square root of the radiator function $H(x, s)$, gives the probability of the emission a photon with an energy fraction of x at the CM energy square s.

Table 8. Canonical input parameters.

m_e	$0.510\,999\,06 \times 10^{-3}$ GeV[15]	m_u	0.0063 GeV [18]	m_Z	91.1876 GeV[15]
m_μ	$105.658\,3389 \times 10^{-3}$ GeV [15]	m_d	0.0063 GeV [18]	m_W	80.366 GeV [18]
m_τ	1.771 GeV[15]	m_c	1.5 GeV [18]	m_H	125.1 GeV[15]
$m_{\nu e}$	0 GeV	m_s	0.0094 GeV [18]	α	1/137.035 999 084[15]
$m_{\nu\mu}$	0 GeV	m_b	4.7 GeV [18]	$\sin^2\theta_W$	$1 - \frac{m_W^2}{m_Z^2}$
$m_{\nu\tau}$	0 GeV	m_t	172.9 GeV [15]	Γ_Z	2.49 GeV [15]

In this method, the electron and positron can emit different energies, and thus the finite boost of the CM system can be treated. The structure function can be obtained as

$$D(1-x,s)^2 = H(x,s) = \Delta_2 \beta x^{\beta-1} - \Delta_1 \beta \left(1 - \frac{x}{2}\right) + \frac{\beta^2}{8}\left[-4(2-x)\log x - \frac{1+3(1-x)^2}{x}\log(1-x) - 2x\right], \tag{10}$$

where

$$\beta = \frac{2\alpha}{\pi}\left(\log\frac{s}{m_e^2} - 1\right),$$
$$\Delta_2 = 1 + \delta_1,\ \Delta_1 = 1 + \delta_1$$
$$\delta_1 = \frac{\alpha}{\pi}\left(\frac{3}{2}\log\frac{s}{m_e^2} + \frac{\pi^2}{3} - 2\right).$$

This result is obtained based on perturbative calculations of initial-state photon emission diagrams up to one-loop order. Reference [17] shows the formula for the $\mathcal{O}(\alpha^2)$ ISR effects. On the other hand, we are interested in separating the $\mathcal{O}(\alpha)$ photonic corrections from the full $\mathcal{O}(\alpha)$ electroweak corrections. It is known that such a separation cannot be realized based on diagrammatic calculations due to the $SU(2)_L \times U(1)$ gauge invariance. On the other hand, the exponentiation method has no such problems estimating the initial-state photonic effects. However, it is exponentiated because we would like to extract $\mathcal{O}(\alpha)$ photonic effects as precisely as possible. We neglect the term δ_2, which is just the term of the $\mathcal{O}(\alpha^2)$ ISR formula in Ref. [17].

6. Results of lepton processes with polarization

A canonical set of the inputs for the electroweak parameters for the numerical evaluations is chosen as shown in Table 8. Here the light quark masses are taken from the numerical program MW.f written by Z. Hioki [18] to reproduce the total hadronic cross sections of e^+e^- collisions in the low-energy regions by means of dispersion relations, and which also calculates the electroweak one-loop corrected m_W from $\alpha, m_Z, m_H, m_e, m_\mu, m_\tau, m_u, m_d, m_s, m_c, m_b$, and m_t as input parameters as $m_W = 80.366$ GeV.

6.1 $e^+e^- \to \mu^+\mu^- H$

Now we are going to show five types of typical one-loop Feynman diagrams with typical three-point functions in Fig. 2, typical four-point and five-point ones in Fig. 3, and a typical fish-type diagrm in Fig. 4, respectively. The treatment of these kinds of n-point Feynman diagrams in GRACE-Loop is discussed in detail in Refs. [7,19].

Table 9 shows the total cross sections of the tree level, those of $\mathcal{O}_\alpha$ corrected with the NOLFS approximation and those including the ISR effects. It shows also the total ratios, $\delta_{\mathcal{O}_\alpha}$ with the

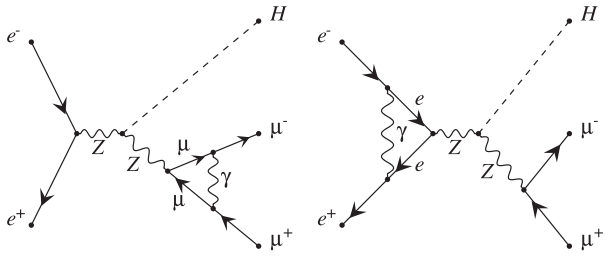

Fig. 2. Typical final and initial vertex correction Feynman diagrams of $e^+e^- \to \mu^+\mu^- H$.

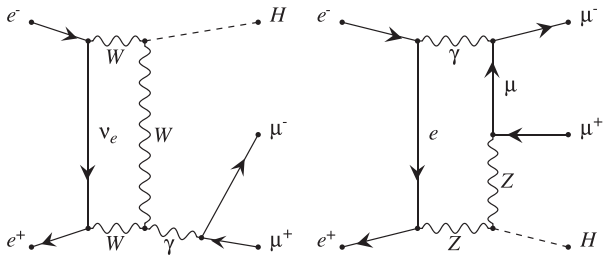

Fig. 3. Typical four- and five-point functions of Feynman diagrams of $e^+e^- \to \mu^+\mu^- H$.

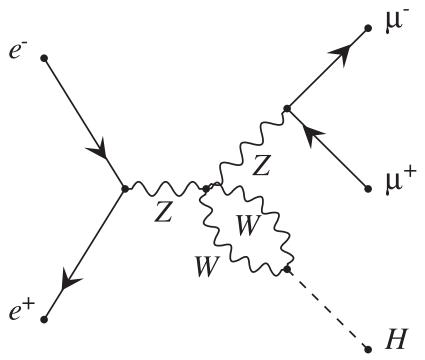

Fig. 4. A typical fish-type Feynman diagram of $e^+e^- \to \mu^+\mu^- H$.

Table 9. The cross section of $e^+e^- \to \mu^+\mu^- H$ with various conditions of beam polarization and without experimental cuts.

	$\sigma_{\rm Tree}$ (pb)	$\sigma_{\mathcal{O}_\alpha}$ (pb)	$\delta_{\rm Total}\%$	$\sigma_{\rm ISR}$ (pb)	$\delta_{\rm ISR}\%$
UP	$7.021(2) \times 10^{-3}$	$6.724(1) \times 10^{-3}$	-4.2	$6.312(4) \times 10^{-3}$	-9.9
RR	$2.16(1) \times 10^{-11}$	$8.4(2) \times 10^{-7}$	3.91×10^{6}	$9.62(3) \times 10^{-13}$	-95.6
LL	$2.16(1) \times 10^{-11}$	$8.45(2) \times 10^{-7}$	3.91×10^{6}	$7(2) \times 10^{-11}$	224.1
RL	$1.108(2) \times 10^{-2}$	$1.194(1) \times 10^{-2}$	7.7	$1.534(3) \times 10^{-3}$	-19.3
LR	$1.709(2) \times 10^{-2}$	$1.497(1) \times 10^{-2}$	-12.1	$9.944(2) \times 10^{-2}$	-9.9
ILC	$1.035(2) \times 10^{-2}$	$9.182(1) \times 10^{-3}$	-11.3	$9.321(4) \times 10^{-3}$	-9.9

NOLFS approximation and $\delta_{\rm ISR}$ with the ISR effects for the various polarization conditions (i.e., UP, RR, LL, RL, LR, and ILC) defined in Sect. 3. The convergence of phase space integration for both the one-loop effects and also the ISR effects is very bad for the LL and RR cases because of the tiny cross section of the tree at $\sim 10^{-11}$ pb due to the very small electron mass effects. However, for the case of the proposed ILC polarization with $p_e = -0.8$, $p_p = 0.3$,

Table 10. The cross section of $e^+e^- \to e^+e^-H$ with various conditions of beam polarization and without experimental cuts.

	$\sigma_{\rm Tree}$ (pb)	$\sigma_{\mathcal{O}_\alpha}$ (pb)	$\delta_{\rm Total}\%$	$\sigma_{\rm ISR}$ (pb)	$\delta_{\rm ISR}\%$
UP	$7.714(2) \times 10^{-3}$	$7.348(1) \times 10^{-3}$	-4.7	$6.314(4) \times 10^{-3}$	-18.1
RR	$6.87(4) \times 10^{-4}$	$6.22(1) \times 10^{-4}$	-9.4	$3.080(2) \times 10^{-4}$	-88.8
LL	$6.87(4) \times 10^{-4}$	$6.22(1) \times 10^{-4}$	-9.4	$3.080(2) \times 10^{-4}$	-55.4
RL	$1.149(2) \times 10^{-2}$	$1.236(1) \times 10^{-2}$	7.6	$9.769(2) \times 10^{-3}$	-15.0
LR	$1.799(3) \times 10^{-2}$	$1.576(1) \times 10^{-2}$	-12.4	$1.487(3) \times 10^{-2}$	-17.3
ILC	$1.119(1) \times 10^{-2}$	$9.841(2) \times 10^{-3}$	-12.0	$9.159(4) \times 10^{-3}$	-18.1

Table 11. The cross section of $e^+e^- \to \tau^+\tau^-H$ with various conditions of beam polarization and without experimental cuts.

	$\sigma_{\rm Tree}$ (pb)	$\sigma_{\mathcal{O}_\alpha}$ (pb)	$\delta_{\rm Total}\%$	$\sigma_{\rm ISR}$ (pb)	$\delta_{\rm ISR}\%$
UP	$7.018(2) \times 10^{-3}$	$6.708(5) \times 10^{-3}$	-4.4	$6.294(4) \times 10^{-3}$	-10.3
RR	$2.10(2) \times 10^{-9}$	$8.44(3) \times 10^{-7}$	4.0×10^4	$8.20(7) \times 10^{-12}$	-99.6
LL	$2.10(2) \times 10^{-9}$	$8.44(3) \times 10^{-7}$	4.0×10^4	$8.3(7) \times 10^{-12}$	-99.6
RL	$1.1078(2) \times 10^{-2}$	$1.189(6) \times 10^{-2}$	7.3	$9.17(2) \times 10^{-3}$	-10.5
LR	$1.7021(4) \times 10^{-2}$	$1.491(1) \times 10^{-2}$	-12.4	$1.524(2)\text{E} \times 10^{-2}$	-10.5
ILC	$1.0343(2) \times 10^{-2}$	$9.145(2) \times 10^{-3}$	-11.6	$9.261(4) \times 10^{-3}$	-10.5

the convergence of the phase space integration is very good and we get reliable numbers at 0.1% accuracy.

6.2 $e^+e^- \to e^+e^-H$

Note that the notations and symbols used for $e^+e^- \to e^+e^-H$ and other processes are the same as those for the $e^+e^- \to \mu^+\mu^-H$ process for UP, RR, LL, RL, LR, and ILC. In this process, because of the sizable t-channel amplitude contribution, $\sigma_{\mathcal{O}_\alpha({\rm ILC})e^+e^-H} = 9.841(2) \times 10^{-3}$ pb is larger than $\sigma_{\mathcal{O}_\alpha({\rm ILC})\mu^+\mu^-H} = 9.182(1) \times 10^{-3}$ pb in Sect. 6.1 by approximately 7% at the proposed ILC with $p_e = -0.8, p_p = 0.3$. Because it is not necessary to form a spin-1 state at the t-channel, the LL and RR cross sections are sizable even at the tree level. Table 10 shows detailed values.

6.3 $e^+e^- \to \tau^+\tau^-H$

There is a question about the tau particle that we are interested in: whether the tau mass can be neglected or not.

$\sigma_{\mathcal{O}_\alpha({\rm ILC})\tau^+\tau^-H} = 9.145(2) \times 10^{-3}$ pb and $\sigma_{\mathcal{O}_\alpha({\rm ILC})\mu^+\mu^-H} = 9.2100(1) \times 10^{-3}$ pb in Sect. 6.1 are quite similar, as expected, because all of the final radiation effects like $\ln\left(\frac{m_\tau^2}{s}\right)$ are canceled according to the Kinoshita–Lee–Nauenberg theorem [20,21]. The terms from the initial-state radiation of $\ln\left(\frac{m_e^2}{s}\right)$ of e^+e^- still remain and have the same effects for both processes of $\tau^+\tau^-H$ and $\mu^+\mu^-H$. More results for the cases of the other polarization conditions are shown in Table 11.

Table 12. The cross section of $e^+e^- \to \nu_\mu \bar{\nu}_\mu H$ with various conditions of beam polarization and without experimental cuts.

	σ_{Tree} (pb)	$\sigma_{\mathcal{O}_\alpha}$ (pb)	$\delta_{\text{Total}}\%$	σ_{ISR} (pb)	$\delta_{\text{ISR}}\%$
UP	$1.3891(6) \times 10^{-2}$	$1.328(3) \times 10^{-2}$	-4.4	$1.249(1) \times 10^{-2}$	-10.1
RR	$2.71(1) \times 10^{-12}$	$1.669(7) \times 10^{-6}$	6.16×10^{7}	$1.971(6) \times 10^{-12}$	-27.3
LL	$2.71(1)) \times 10^{-12}$	$1.669(7) \times 10^{-6}$	6.15×10^{7}	$2.307(7) \times 10^{-12}$	-14.9
RL	$2.191(1) \times 10^{-2}$	$2.409(7) \times 10^{-2}$	10.0	$1.965E(1) \times 10^{-2}$	-10.3
LR	$3.367(1) \times 10^{-2}$	$2.905(1) \times 10^{-2}$	13.7	$3.022(1) \times 10^{-2}$	-10.2
ILC	$2.045(1) \times 10^{-2}$	$1.782(1) \times 10^{-2}$	-12.9	$1.837(1) \times 10^{-2}$	-10.2

Table 13. The cross section of $e^+e^- \to \nu_e \bar{\nu}_e H$ with various conditions of beam polarization and without experimental cuts.

	σ_{Tree} (pb)	$\sigma_{\mathcal{O}_\alpha}$ (pb)	$\delta_{\text{Total}}\%$	σ_{ISR} (pb)	$\delta_{\text{ISR}}\%$
UP	$2.067(1) \times 10^{-2}$	$2.002(9) \times 10^{-2}$	-3.1	$1.764(2) \times 10^{-2}$	-14.6
RR	$3.05(2) \times 10^{-12}$	$3.53(2) \times 10^{-6}$	1.16×10^{8}	$2.043(8) \times 10^{-12}$	-33.0
LL	$3.05(2) \times 10^{-12}$	$3.53(2) \times 10^{-6}$	1.16×10^{8}	$2.385(9) \times 10^{-12}$	-21.8
RL	$2.191(1)) \times 10^{-2}$	$2.414(7) \times 10^{-2}$	10.2	$1.905(1) \times 10^{-2}$	-10.3
LR	$6.076(1)) \times 10^{-2}$	5.612×10^{-2}	-7.6	$5.085(2) \times 10^{-2}$	-16.3
ILC	$3.632(1)) \times 10^{-2}$	$3.357(3) \times 10^{-2}$	-7.6	$3.044(2) \times 10^{-2}$	-16.2

Table 14. The cross section of $e^+e^- \to u\bar{u}H$ with various conditions of beam polarization and without experimental cuts.

	σ_{Tree} (pb)	$\sigma_{\mathcal{O}_\alpha}$ (pb)	$\delta_{\text{Total}}\%$	σ_{ISR} (pb)	$\delta_{\text{ISR}}\%$
UP	$2.424(1) \times 10^{-2}$	$2.258(2) \times 10^{-2}$	-6.8	$2.178(2) \times 10^{-2}$	-10.1
RR	$3.65(2) \times 10^{-11}$	$2.915(1) \times 10^{-6}$	7.98×10^{6}	$8(4) \times 10^{-11}$	11.9
LL	$3.65(2) \times 10^{-11}$	$2.92(1) \times 10^{-6}$	7.98×10^{6}	$8(4) \times 10^{-11}$	11.9
RL	$3.824(1) \times 10^{-2}$	$4.32(1) \times 10^{-2}$	13.1	$3.431(1) \times 10^{-2}$	-10.0
LR	$5.875(1) \times 10^{-2}$	$4.809(1) \times 10^{-2}$	-18.2	$5.274(1) \times 10^{-2}$	-10.0
ILC	$3.570(1) \times 10^{-2}$	$2.934(1) \times 10^{-2}$	-17.8	$3.206(2) \times 10^{-2}$	-10.0

6.4 $e^+e^- \to \nu_\mu \bar{\nu}_\mu H$

The difference between δ_{Total} and δ_{ISR} is approximately 5%. We skip the $e^+e^- \to \nu_\tau \bar{\nu}_\tau H$ process because it is quite similar to this one. More results are provided in Table 12.

6.5 $e^+e^- \to \nu_e \bar{\nu}_e H$

$e^+e^- \to \nu_e \bar{\nu}_e H$ has a t-channel. Table 13 shows the results of the $e^+e^- \to \nu_e \bar{\nu}_e H$ process.

7. Results of quark processes

7.1 $e^+e^- \to u\bar{u}H$

QCD corrections up to four-loop level are well known, and with just in one-loop corrections is popular as the simple factor of $1 + \frac{\alpha_s}{\pi} \simeq 1.03\%$, where α_s is the coupling constant of the strong interaction ($\alpha_s \simeq 1/10$); thus we will not discuss it in this paper. Table 14 shows the calculation results of the first quark process $e^+e^- \to u\bar{u}H$.

Table 15. The cross section of $e^+e^- \to d\bar{d}H$ with various conditions of beam polarization and without experimental cuts.

	$\sigma_{\rm Tree}$ (pb)	$\sigma_{\mathcal{O}_\alpha}$ (pb)	$\delta_{\rm Total}\%$	$\sigma_{\rm ISR}$ (pb)	$\delta_{\rm ISR}\%$
UP	$3.112(1) \times 10^{-2}$	$2.961(1) \times 10^{-2}$	-4.8	2.796×10^{-2}	-10.2
RR	$1.40(1) \times 10^{-11}$	$3.74(2) \times 10^{-6}$	2.7×10^{-7}	$1.9(8) \times 10^{-10}$	1257
LL	$1.40(1) \times 10^{-11}$	$3.74(2) \times 10^{-6}$	2.7×10^{-7}	$1.8(8) \times 10^{-10}$	1186
RL	$4.907(1) \times 10^{-2}$	$5.205(1) \times 10^{-2}$	6.1	$6.769(2) \times 10^{-2}$	-10.6
LR	$7.567(1) \times 10^{-2}$	$6.650(1) \times 10^{-2}$	-12.1	$4.402(2) \times 10^{-2}$	-10.3
ILC	$4.581(1) \times 10^{-2}$	$4.070(6)\mathrm{E} \times 10^{-2}$	-11.5	$4.115(2) \times 10^{-2}$	-10.2

Table 16. The cross section of $e^+e^- \to c\bar{c}H$ with various conditions of beam polarization and without experimental cuts.

	$\sigma_{\rm Tree}$ (pb)	$\sigma_{\mathcal{O}_\alpha}$ (pb)	$\delta_{\rm Total}\%$	$\sigma_{\rm ISR}$ (pb)	$\delta_{\rm ISR}\%$
UP	$2.421(1) \times 10^{-2}$	$2.259(1) \times 10^{-2}$	-6.8	$2.175(2) \times 10^{-2}$	-10.2
RR	$1.482(7) \times 10^{-11}$	$2.91(1) \times 10^{-6}$	1.96×10^{7}	$1.4155(8) \times 10^{-11}$	-4.9
LL	$1.482(7) \times 10^{-11}$	$2.91(1) \times 10^{-6}$	1.96×10^{7}	$1.4600(8) \times 10^{-11}$	-1.5
RL	$3.819(1) \times 10^{-2}$	$4.300(1) \times 10^{-2}$	12.6	$3.425(2) \times 10^{-2}$	-10.3
LR	$5.890(1) \times 10^{-2}$	$4.771(1) \times 10^{-2}$	-19.0	$5.266(1) \times 10^{-2}$	-10.6
ILC	$3.566(1) \times 10^{-2}$	$2.926(4) \times 10^{-2}$	-18.0	$3.202(2) \times 10^{-2}$	-10.2

Table 17. The cross section of $e^+e^- \to b\bar{b}H$ with various conditions of beam polarization and without experimental cuts.

	$\sigma_{\rm Tree}$ (pb)	$\sigma_{\mathcal{O}_\alpha}$ (pb)	$\delta_{\rm Total}\%$	$\sigma_{\rm ISR}$ (pb)	$\delta_{\rm ISR}\%$
UP	$3.078(1) \times 10^{-2}$	$2.88(1) \times 10^{-2}$	-6.3	$2.765(2) \times 10^{-2}$	-10.2
RR	$7.40(4) \times 10^{-12}$	$3.69(2) \times 10^{-6}$	5.0×10^{7}	$5.70(3) \times 10^{-12}$	-22.9
LL	$7.40(4) \times 10^{-12}$	$3.69(2) \times 10^{-6}$	5.0×10^{7}	$6.31(3) \times 10^{-12}$	-14.6
RL	$4.855(1) \times 10^{-2}$	$5.06(1) \times 10^{-2}$	4.2	$4.035(1) \times 10^{-2}$	-10.2
LR	$7.461(2) \times 10^{-2}$	$6.46(1) \times 10^{-2}$	-13.5	$6.691(2 \times 10^{-2}$	-10.2
ILC	$4.533(1) \times 10^{-2}$	$3.969(4) \times 10^{-2}$	-12.5	$4.068(2)\mathrm{E} \times 10^{-2}$	-10.3

7.2 $e^+e^- \to d\bar{d}H$

The isospin of the u quark is up while that of the d quark is down, which explains the difference between $\sigma_{\mathcal{O}_\alpha(\mathrm{ILC})d\bar{d}H} = 4.070(6) \times 10^{-2}$ pb and $\sigma_{\mathcal{O}_\alpha(\mathrm{ILC})u\bar{u}H} = 2.948(4) \times 10^{-2}$ pb as in Sect. 7.1. Table 15 shows the results of the $e^+e^- \to d\bar{d}H$ process.

7.3 $e^+e^- \to c\bar{c}H$

Table 16 shows the cross sections of $e^+e^- \to c\bar{c}H$. The mass of the charm quark is 1.5 GeV and the mass of the up quark is 58 MeV. Because there is no large mass effect from the final-state radiation, the results are quite similar, as expected. Because of this observation, we skip the $e^+e^- \to s\bar{s}H$ process because it has the same characteristics as the $e^+e^- \to d\bar{d}H$ process.

7.4 $e^+e^- \to b\bar{b}H$

Table 17 summarizes the cross sections of $e^+e^- \to b\bar{b}H$. We keep the bottom-Yukawa coupling with the NOLFS approximation for $e^+e^- \to b\bar{b}H$ but not for the other processes. Let us com-

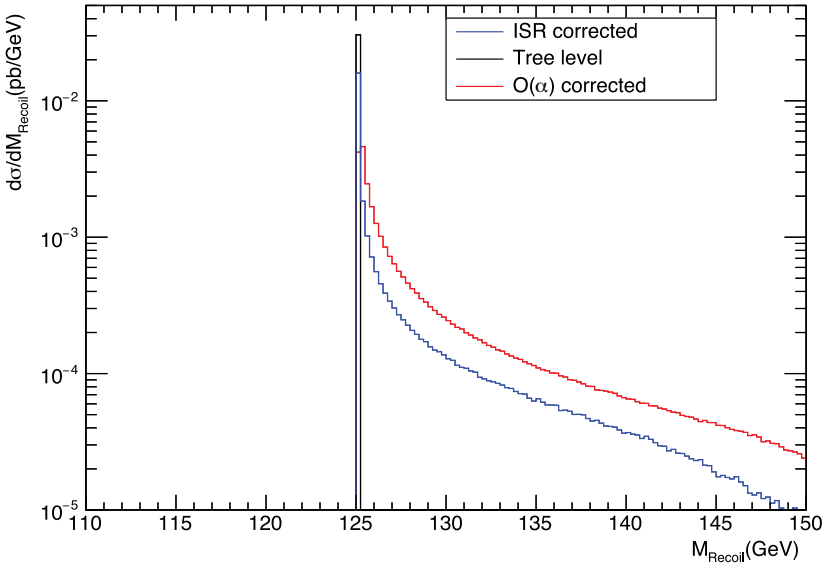

Fig. 5. Recoil mass distribution of $e^+e^- \to \mu^+\mu^- H$ after applying the experimental cuts as in Eqs. (11)–(13) at $\sqrt{s} = 250$ GeV. The bin width is 0.3 GeV.

pare the results of $e^+e^- \to d\bar{d}H$ and $e^+e^- \to b\bar{b}H$ for the proposed ILC, $p_e = -0.8, p_p = 0.3$ at $\delta_{\text{Total(ILC)}}$, which are -11.5% and 12.5%, respectively. This 1% difference is caused by the bottom-Yukawa coupling. With ISR, the results for $e^+e^- \to d\bar{d}H$ and $e^+e^- \to b\bar{b}H$ are quite similar, as expected. This difference between $\delta_{\text{Total(ILC)}}$ and $\delta_{\text{ISR(ILC)}}$ is very interesting. Because this 1% difference originates from the bottom-Yukawa coupling of the bottom quark, it may be hard to observe at the experiments.

8. Recoil mass distribution of $e^+e^- \to \mu^+\mu^- H$ with beam polarization effects

In this section, we discuss the ZH recoil mass distribution $ZH \to \mu^+\mu^- H$ with $\mathcal{O}(\alpha)$ corrections and beam polarization effects. To conduct a more realistic analysis, we apply the following three experimental cuts:

(1) The angular cuts on $\theta_{\mu^+}, \theta_{\mu^-}$,

$$10^\circ < \theta_{\mu^+}, \theta_{\mu^-} < 170^\circ, \tag{11}$$

where θ_{μ^+} and θ_{μ^-} are the scattering angles of the anti-muon and muon, respectively.

(2) The energy cuts on E_{μ^+}, E_{μ^-},

$$E_{\mu^+}, E_{\mu^-} > 10 \text{ GeV}, \tag{12}$$

where E_{μ^+} and E_{μ^-} are the energies of the anti-muon and muon, respectively.

(3) The invariant mass cut $M_{\mu^+\mu^-}$,

$$m_Z - 3\Gamma_Z < M_{\mu^+\mu^-} < m_Z + 3\Gamma_Z, \tag{13}$$

where $M_{\mu^+\mu^-}$ is the invariant mass of the anti-muon and muon particles; $\Gamma_Z = 2.49$ GeV [15] is the width of the Z boson.

Table 18. Summary table of cross sections and total ratios of $e^+e^- \to \mu^+\mu^- H$ with experimental cuts and with the proposed ILC polarization with $p_e = -0.8$, $p_p = 0.3$.

σ_{Tree} (pb)	$\sigma_{\mathcal{O}_\alpha}$ (pb)	σ_{ISR} (pb)	$\delta_{\text{Total}}\%$	$\delta_{\text{ISR}}\%$
$9.143(1) \times 10^{-3}$	$7.910(1) \times 10^{-3}$	$8.236(4) \times 10^{-3}$	-13.2	-9.9

Next, we present the results of the ZH recoil mass distribution with the $\mathcal{O}(\alpha)$ corrections of $e^+e^- \to \mu^+\mu^- H$ at $\sqrt{s} = 250$ GeV, after applying the three types of experimental cuts as defined above. The recoil mass distribution is shown in Fig. 5.

The black line shows the tree-level distribution, the blue line shows the ISR-corrected distribution and the red line shows the $\mathcal{O}(\alpha)$-corrected distribution. The black line only shows one bin peak, the position of which indicates the mass of the Higgs boson. On including the $\mathcal{O}(\alpha)$ corrections, a tail structure appears owing to the ISR effects, which is called the radiative tail. The height of the peak is substantially reduced owing to the one-photon emission effect. However, when the ISR effects are included, the height of the peak increases again because of the higher-order radiation effect. This swing-back effect can occasionally be seen when comparing higher-order and $\mathcal{O}(\alpha)$ corrections.

After applying the three experimental cuts, we obtained the total cross sections and ratios at $\mathcal{O}(\alpha)$ and also those including ISR effects, as shown in Table 18

9. Discussion

First, we discuss the behavior of high-order corrections for the $e^+e^- \to \mu^+\mu^- H$ process in detail. For this process, various conditions of beam polarization without experimental cuts are shown in Table 9. At the tree level, the cross sections corresponding to RR and LL are negligibly small compared with those of RL and LR since RR and LL polarizations cannot produce spin-1 bosons. Small cross sections of RR and LL polarizations result from the spin-flip effect and are proportional to $|\frac{me^2}{s}| \propto \left(\frac{10^{-3}}{10^2}\right)^2 \sim 10^{-10}$. These results are consistent with $\frac{\text{LL+RR}}{\text{LR+RL}} \sim 10^{-11}$. Moreover, $\sigma_{\mathcal{O}_\alpha}$ gives sizeable cross sections on RR and LL polarizations, because the $\mathcal{O}_\alpha$ amplitude includes spin-flip diagrams of the initial-state radiation. Although the cross sections of LL and RR at the tree level are very small, very large total ratios $\delta_{\text{Total}} \sim 10^6$ are observed.

$\sigma_{\mathcal{O}_\alpha(\text{ILC})\mu^+\mu^- H} = 9.182(1) \times 10^{-2}$ pb is larger than $\sigma_{\mathcal{O}_\alpha(\text{UP})\mu^+\mu^- H} = 6.724(1) \times 10^{-3}$ pb thanks to the advantages of the beam polarization of the linear collider. It has significantly better statistics for Higgs with the same luminosity.

Next, we discuss the effect of higher-order corrections on weak interactions and photonic interactions. Note that $\sigma_{\mathcal{O}_\alpha}$ includes both QED and weak corrections. However, it is impossible in general to clearly separate these two effects. We calculated δ_{ISR} as an approximation for QED corrections because ISR corrections dominate over all QED corrections. In this approximation, the weak corrections can be estimated as $\sigma_{\text{weak}} = \sigma_{\mathcal{O}_\alpha} - \sigma_{\text{ISR}}$. $\delta_{\text{ISR(RL)}}$ and $\delta_{\text{ISR(LR)}}$ were obtained to be -19.3% and -9.9%, respectively; however, $\delta_{\text{Total(RL)}} = 7.7\%$ and $\delta_{\text{Total(LR)}} = -12.1\%$. Thus the pure weak correction corresponding to RL is 27% but that corresponding to LR is only -2%. From these results, it is clear that experiments with beam polarization need precise calculations of the electroweak $\sigma_{\mathcal{O}_\alpha}$ corrections. $\delta_{\text{Total(ILC)}} = -11.3\%$, $\delta_{\text{ISR(ILC)}} = -9.9\%$, and the weak correction for the proposed ILC polarization, $p_e = -0.8, p_p = 0.3$, is approximately -1%. This result is sufficient to motivate the ILC to consider the contribution of the pure weak

Table 19. Lepton processes with the proposed ILC beam polarization with $p_e = -0.8, p_p = 0.3$ at $\sqrt{s} =$ 250 GeV and without experimental cuts.

Process	σ_{Tree} (pb)	$\sigma_{\mathcal{O}_\alpha}$ (pb)	$\delta_{\text{Total}}\%$	σ_{ISR} (pb)	$\delta_{\text{ISR}}\%$
$\mu^+\mu^- H$	$1.035(2) \times 10^{-2}$	$9.182(1) \times 10^{-3}$	-11.3	$9.321(4) \times 10^{-3}$	-9.9
$e^+e^- H$	$1.119(1) \times 10^{-2}$	$9.841(2) \times 10^{-3}$	-12.0	$9.159(4) \times 10^{-3}$	-18.1
$\tau^+\tau^- H$	$1.034(1) \times 10^{-2}$	$9.145(2) \times 10^{-3}$	-11.6	$9.261(4) \times 10^{-3}$	-10.5
$\nu_\mu \bar{\nu}_\mu H$	$2.045(1) \times 10^{-2}$	$1.782(1) \times 10^{-2}$	-12.9	$1.837(1) \times 10^{-2}$	-10.2
$\nu_e \bar{\nu}_e H$	$3.632(1) \times 10^{-2}$	$3.357(3) \times 10^{-2}$	-7.6	$3.044(2) \times 10^{-2}$	-16.2

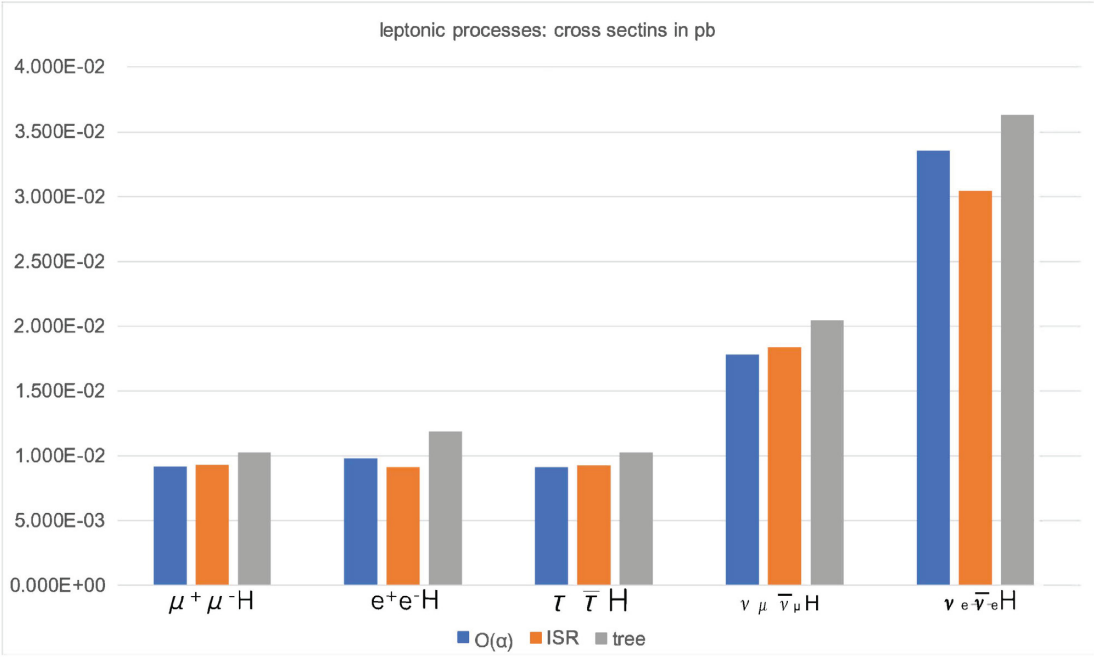

Fig. 6. Cross sections of the leptonic processes with the proposed ILC beam polarization, $p_e = -0.8, p_p = 0.3$ at $\sqrt{s} = 250$ GeV and without experimental cuts.

correction. Additionally, δ_{weak} is necessary to compare with the naive estimation from the running alpha effects of $+14\% = (+7)\% + (+7)\%$.

We have summarized the lepton processes $e^+e^- \to f\bar{f}H$ (i.e., $\mu^+\mu^- H$, $e^+e^- H$, $\tau^+\tau^- H$, $\nu_\mu \bar{\nu}_\mu H$, and $\nu_e \bar{\nu}_e H$) in Table 19.

We present two separate figures for the cross sections and total ratios, for convenience. Figure 6 shows the cross sections at the tree level, as well as $\sigma_{\mathcal{O}_\alpha}$, and ISR cross sections. Figure 7 shows δ_{Total} and δ_{ISR} for the four leptonic processes.

Owing to the sizable contribution of the t-channel amplitude, $\sigma_{\mathcal{O}_\alpha(\text{ILC})\nu_e\bar{\nu}_e H} = 3.632(1) \times 10^{-2}$ pb is larger than $\sigma_{\mathcal{O}_\alpha(\text{ILC})\nu\mu\bar{\nu}_\mu H} = 1.782(1) \times 10^{-2}$ pb. $\delta_{\text{Total(ILC)}\nu_\mu\bar{\nu}_\mu H} = -12.9\%$ and $\delta_{\text{ISR(ILC)}\nu_\mu\bar{\nu}_\mu H} = -10.2\%$, and hence the pure weak correction for $\nu_\mu \bar{\nu}_\mu H$ is approximately -3%, whereas $\delta_{\text{Total(ILC)}\nu_e\bar{\nu}_e H} = -7.6\%$ and $\delta_{\text{ISR(ILC)}\nu_e\bar{\nu}_e H} = -16.2\%$; hence, the pure weak correction for $\nu_e \bar{\nu}_e H$ is approximately $+9\%$. Moreover, $\mu^+\mu^- H$ and $e^+e^- H$ have the same tendency as $\nu_\mu \bar{\nu}_\mu H$ and $\nu_e \bar{\nu}_e H$. From this discussion, it is clear that, although the t-channel cross sections at tree level are small, they are important for $\delta_{\text{Total(ILC)}\nu_\mu\bar{\nu}_\mu H} = -12.9\%$ and

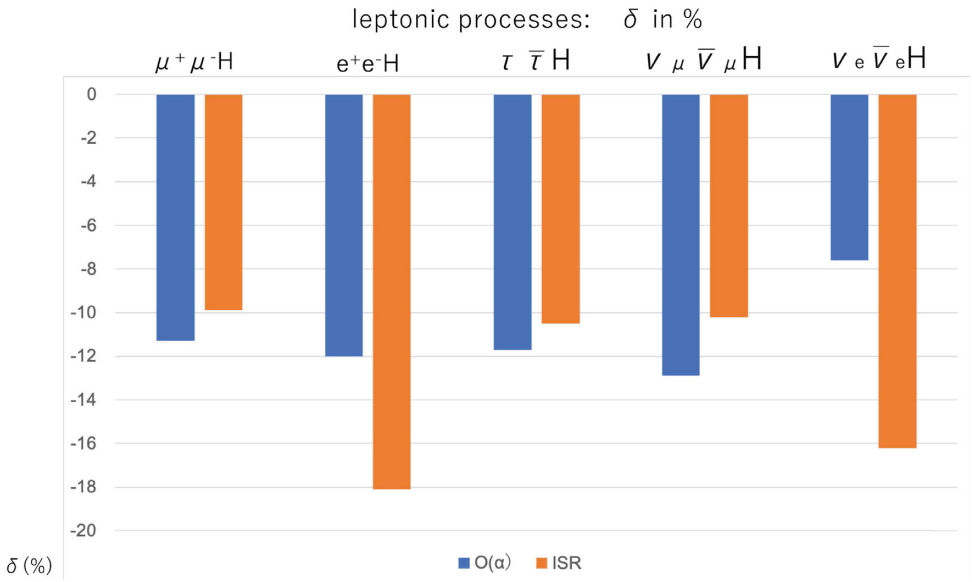

Fig. 7. Ratios of the leptonic processes with the proposed ILC beam polarization, $p_e = -0.8, p_p = 0.3$ at $\sqrt{s} = 250$ GeV and without experimental cuts.

Table 20. Quark processes with the proposed ILC beam polarization, $p_e = -0.8, p_p = 0.3$ at $\sqrt{s} = 250$ GeV and without experimental cuts.

Process	σ_{Tree} (pb)	$\sigma_{\mathcal{O}_\alpha}$ (pb)	$\delta_{\text{Total}}\%$	σ_{ISR} (pb)	$\delta_{\text{ISR}}\%$
$u\bar{u}H$	$3.570(1) \times 10^{-2}$	$2.934(1) \times 10^{-2}$	-17.8	$3.206(2) \times 10^{-2}$	-10.0
$d\bar{d}H$	$4.581(1) \times 10^{-2}$	$4.070(1) \times 10^{-2}$	-11.5	$4.115(2) \times 10^{-2}$	-10.2
$c\bar{c}H$	$3.566(1) \times 10^{-2}$	$2.926(1) \times 10^{-2}$	-18.0	$3.215(2) \times 10^{-2}$	-10.2
$b\bar{b}H$	$4.533(1) \times 10^{-2}$	$3.969(4) \times 10^{-2}$	-12.5	$4.068(2) \times 10^{-2}$	-10.3

$\delta_{\text{Total(ILC)}\nu_e\bar{\nu}_e H} = -7.6\%$; this 5.3% difference may be a result of the charge/neutral channel or isospin up/down type.

Next, we discuss the quark processes $e^+e^- \to f\bar{f}H$ (i.e., $u\bar{u}H$, $d\bar{d}H$, $c\bar{c}H$, $b\bar{b}H$), which are summarized in Table 20.

Again, we present two separate figures for the cross sections and total ratios. Figure 8 shows the cross sections at the tree level as well as the $\sigma_{\mathcal{O}_\alpha}$ and ISR cross sections. Figure 9 shows δ_{Total} and δ_{ISR} for the four quark processes.

δ_{ISR} is approximately -10% for all processes.

δ_{Total} of the up-type quarks is -18%, while δ_{Total} of the down-type quarks is -12% because of the charge difference or up/down type with different isospins.

$\sigma_{\mathcal{O}_\alpha\text{(ILC)}u\bar{u}H} = 2.933(4) \times 10^{-2}$ pb is larger than $\sigma_{\mathcal{O}_\alpha\text{(ILC)}c\bar{c}H} = 2.926(4) \times 10^{-2}$ pb as expected. These exhibit the opposite tendency to leptons.

$\delta_{\text{Total(ILC)}d\bar{d}H} = -11.5\%$ and $\delta_{\text{Total(ILC)}b\bar{b}H} = -12.5$, with the 1% difference arising because of the Yukawa coupling. Weak corrections for the up-type and down-type quarks are approximately -8% and -2%, respectively.

Next, we compare the lepton and quark channels. For leptons, δ_{ISR} values for s-channel and t-channel processes approximate -10% and -18%, respectively; for quarks, δ_{ISR} is approximately -10% for all the cases with the ILC polarized beams and without experimental cuts.

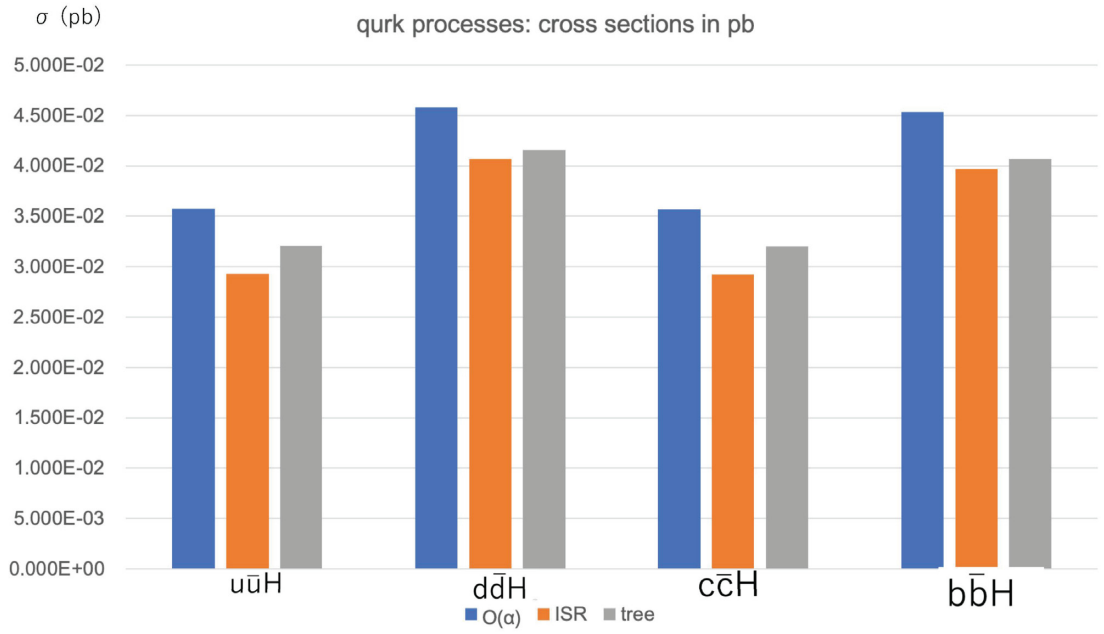

Fig. 8. Cross sections of the quark processes with the proposed ILC beam polarization, $p_e = -0.8, p_p = 0.3$ at $\sqrt{s} = 250$ GeV and without experimental cuts.

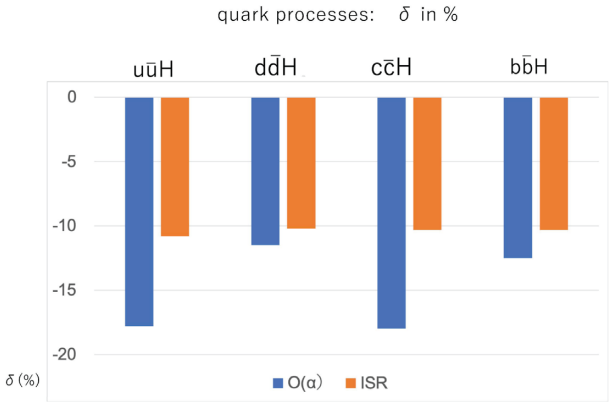

Fig. 9. Ratios of the quark processes with the proposed ILC beam polarization $p_e = -0.8, p_p = 0.3$ at $\sqrt{s} = 250$ GeV and without experimental cuts.

Comparing the lepton and quark channels, the difference between the up- and down-types is clearly observed in quarks; however, this is not observed for leptons.

We also calculated the recoil mass distribution after applying three experimental cuts for the $e^+e^- \to \mu^+\mu^- H$ process at the $\mathcal{O}(\alpha)$ corrections and including the ISR effects. The following results were obtained: $\delta_{\text{Total}} = -13.2\%$ and $\delta_{\text{ISR}} = -9.9\%$, such that the weak correction was estimated to be -3%. Thus, to measure the g_{HZZ} coupling within 1% accuracy, the weak correction of -3% cannot be neglected.

10. Conclusion

We have presented the full $\mathcal{O}(\alpha)$ electroweak radiative corrections to nine associated Higgs fermion pair production processes in e^+e^- collisions with beam polarization at the International Linear Collider (ILC). The computation was performed with the help of GRACE-loop.

We compared the full $\mathcal{O}(\alpha)$ electroweak radiative corrections with the factorized initial-state radiation (ISR) effects to estimate the pure weak corrections. The matrix element to be produced by GRACE-loop was tested by (1) renormalization, (2) infrared divergence-free regularization, (3) hard photon cut parameter (k_c) independence in 0.1%, and (4) independence of the non-linear gauge parameters.

Our calculations have the following features: (1) the beam polarization effect was considered, (2) the mass effect of all the fermions except neutrinos was retained, and (3) Yukawa coupling of the bottom quark was included. To the best of our knowledge, this is the first detailed discussion of the $e^+e^- \to f\bar{f}H$ processes. Furthermore, we compared our results with those of multiple photon emission from electrons and positrons in the ISR process and highlighted that the $\mathcal{O}(\alpha)$ corrections presented in this work are important for the analysis of experimental data. In the case of the $e^+e^- \to \mu^+\mu^- H$ process with the experimental cuts and the proposed ILC beam polarization condition, the pure weak correction was estimated to be -3%. Thus, in order to measure the g_{HZZ} coupling within 1% accuracy, the pure weak $\mathcal{O}(\alpha)$ corrections cannot be neglected.

Acknowledgments

This paper is based on the Ph.D. thesis of N.M.U.Q. in 2021 [22]. This work is part of the collaboration of the Minami-Tateya group at IPNS from KEK. We acknowledge useful discussions with T. Kaneko and F. Yuasa from KEK and their continuous encouragement. J.F. and N.M.U.Q. especially acknowledge Z. Hioki for supplying the Fortran program MW.f and the best-recommended values of the light-quark masses to calculate the electroweak $\mathcal{O}(\alpha)$ corrections of the mass of the W boson. N.M.U.Q. would also like to acknowledge Tran Thanh Van for his help after getting her Ph.D. Y.K. appreciates the warm hospitality of members of the Nikhef theory group, especially J. Vermaseren and E. Laenen. He started the first calculation of this study during his stay at Nikhef.

Funding

Open Access funding: SCOAP[3].

References

[1] T. Behnke, J. E. Brau, B. Foster, J. Fuster, M. Harrison, J. McEwan Paterson, M. Peskin, M. Stanitzki, N. Walker, and H. Yamamoto, arXiv:1306.6327 [physics.acc-ph] [Search INSPIRE].
[2] K. Fujii, arXiv:1305.1692 [hep-ex] [Search INSPIRE].
[3] G. Aad et al., Phys. Lett. B **716**, 1 (2012).
[4] S. Chatrchyan et al., Phys. Lett. B **716**, 30 (2012).
[5] GRACE home page (2022) (available at: https://minami-home.kek.jp/).
[6] J. A. M. Vermaseren, arXiv:math-ph/0010025 [Search INSPIRE].
[7] G. Bélanger, F. Boudjema, J. Fujimoto, T. Ishikawa, T. Kaneko, K. Kato, and Y. Shimizu, Phys. Rep. **430**, 117 (2006).
[8] G. Bélanger, F. Boudjema, J. Fujimoto, T. Ishikawa, T. Kaneko, K. Kato, and Y. Shimizu, Phys. Lett. B **559**, 252 (2003).
[9] A. Denner, S. Dittmaier, M. Roth, and M. M. Weber, Nucl. Phys. B **660**, 289 (2003).
[10] J. Fujimoto, T. Ishikawa, M. Jimbo, T. Kon, Y. Kurihara, and M. Kuroda, Phys. Rev. D **75**, 113002 (2007).
[11] K. Aoki, Z. Hioki, R. Kawabe, M. Konuma, and T. Muta, Prog. Theor. Phys. Suppl. **73**, 1 (1982).
[12] T. Hahn and M. Pérez-Victoria, Comput. Phys. Commun. **118**, 153 (1999).
[13] F. Boudjema and E. Chopin, Z. Phys. C **73**, 85 (1996).
[14] S. Kawabata, Comput. Phys. Commun. **88**, 309 (1995).
[15] M. Tanabashi et al., Phys. Rev. D **98**, (2018).
[16] M. E. Peskin, K. Fujii, and C. Grojean, arXiv:1710.07621v4 [hep-ex] [Search INSPIRE].

[17] J. Fujimoto, Y. Kurihara, and N. M.U. Quach, Eur. Phys. J. C **79**, 506 (2019).
[18] Z. Hioki, Prog. Theor. Phys. **68**, 2134 (1982).
[19] H. K. Phan, Ph.D. Thesis, SOKENDAI (2014).
[20] T. Kinoshita, J. Math. Phys. **3**, 650 (1962).
[21] T. D. Lee and M. Nauenberg, Phys. Rev. **133**, B1549 (1964).
[22] N. M. U. Quach, Beam polarization effects on Higgs boson production at the International Linear Collider, Ph.D. Thesis (2021) (available at: http://id.nii.ac.jp/1013/00006095/).